



ELSEVIER

Contents lists available at ScienceDirect

## Biosensors and Bioelectronics

journal homepage: [www.elsevier.com/locate/bios](http://www.elsevier.com/locate/bios)

# Development of a novel electrochemical DNA biosensor based on elongated hexagonal-pyramid CdS and poly-isonicotinic acid composite film



Delun Zheng, Qingxiang Wang\*, Feng Gao, Qinghua Wang, Weiwei Qiu, Fei Gao

Department of Chemistry and Environment Science, Fujian Province University Key Laboratory of Analytical Science, Minnan Normal University, Zhangzhou 363000, PR China

## ARTICLE INFO

## Article history:

Received 14 January 2014

Received in revised form

3 April 2014

Accepted 4 April 2014

Available online 18 April 2014

## Keywords:

Elongated hexagonal-pyramid CdS

Isonicotinic acid

Electrochemical polymerization

DNA biosensor

## ABSTRACT

Three CdS materials with different shapes (i.e., irregular, rod-like, and elongated hexagonal-pyramid) were hydrothermally synthesized through controlling the molar ratio of  $\text{Cd}^{2+}$  to thiourea. Electrochemical experiments showed that the elongated hexagonal-pyramid CdS (eh-CdS) modified on glassy carbon electrode (GCE) had the higher electrical conductivity than the other two forms. Then the eh-CdS modified GCE was further modified with a layer of poly-isonicotinic acid (PIA) through electropolymerization in IA solution to enhance the stability and functionality of the interface. The layer-by-layer modification process was characterized by atomic force microscopy and electrochemistry. Then 5'-amino functionalized DNA was immobilized on the electrode surface through coupling with the carboxylic groups derived from PIA-eh-CdS composite film. The hybridization performance of the developed biosensor was evaluated using methylene blue as redox indicator, and the results showed that the peak currents of methylene blue varied with target concentrations in a wide linear range from  $1.0 \times 10^{-14}$  M to  $1.0 \times 10^{-9}$  M with a low detection limit of  $3.9 \times 10^{-15}$  M. The biosensor also showed high stability and good discrimination ability to the one-base, three-base mismatched and non-complementary sequence.

© 2014 Elsevier B.V. All rights reserved.

## 1. Introduction

Specific DNA detection has become a most important research field due to its potential application in food safety and quality monitoring, disease diagnosis, drug screening, epidemic prevention and environmental protection. Among the various DNA detection technologies, the electrochemical method attracted considerable interest in both theoretical and practical aspects because of its simplicity, rapidness, low-cost and easiness to miniaturize (Wan et al., 2010; Xuan et al., 2012; Lou et al., 2013). During fabrication of an electrochemical DNA biosensor, the preparation of an appropriate interface for the probe DNA immobilization is a critical step, since it can significantly influence the biosensor's multiple performance such as accuracy, sensitivity, selectivity and lifetime.

With the development of the nanoscience, various kinds of the nano-scaled materials have been utilized as a supporting platform for DNA immobilization due to their unique characteristics such as large surface area, high electrical conductivity, excellent biocompatibility

and strong adsorption ability (Du et al., 2009; Zhang et al., 2010; Liu et al., 2013). Cadmium sulfide (CdS), as one of the most important binary semiconductor, has been extensively studied in the fields of sensors, solar cells, field-effect transistors, electricity generation and light-emitting diodes (Miao et al., 2008; Huang et al., 2005; Ameen et al., 2012). Owing to its excellent electrical conductivity, the nano-sized CdS has also been frequently used as the electrode materials in electrochemical sensors. For example, Qian et al. (2012) have immobilized glucose oxidase on a hexagonally faced CdS nanorod array, which resulted in a glucose biosensor with high enzyme loading and excellent sensitivity. Ferancová et al. (2010) have prepared a composite containing pear-like CdS and chitosan for trace determination of guanine and adenine bases in DNA, through which the DNA damage could be successfully monitored. The CdS-based electrochemical sensors for the other analytes such as  $\text{Hg}^{2+}$  (Long et al., 2009), thrombin (Wang et al., 2011a), and nitrate (Fang et al., 2009) have also been reported.

On the other hand, as an inorganic nanomaterial, the lack of organic groups on the surface of CdS particles decreases their stability and affinity with the basal interface, and more importantly, suppressed their ability to immobilize biological molecules through the favorable covalent bond. In order to overcome these

\* Corresponding author. Tel.: +86 596 2591445; fax: +86 596 2520035.

E-mail address: [axiang236@126.com](mailto:axiang236@126.com) (Q. Wang).

deficiencies, some organic polymers are usually introduced. Electropolymerization is one of the most popular approaches because the thickness, permeation, character and functionality of the film can be well controlled by this method (Peng et al., 2009; Xue et al., 2005). Isonicotinic acid (IA) is an important pyridine derivative used in the manufacture of isoniazid (antituberculosatic drug) and other pharmaceutically important drugs. Recently poly-isonicotinic acid (PIA) modified electrodes have been utilized in the electroanalysis of a variety of biomolecules such as dopamine, norepinephrine, ascorbic acid and glucose (Zhu and Lin, 2009; Ojani et al., 2011; Zhao et al., 2002). However, the application of PIA as a platform for DNA immobilization and hybridization detection has not been reported yet.

In this paper, three kinds of CdS nanoparticles with different shapes were hydrothermally synthesized through tuning the ratio of  $\text{Cd}^{2+}$  to thiourea (TU). Then the elongated hexagonal-pyramid CdS (eh-CdS) nanoparticle was selected for the modification of glassy carbon electrode (GCE) because it has the higher electrocatalytic capacity than the other two forms. Followed by, a layer of organic PIA film was grown on the eh-CdS modified electrode to improve the stability and the functionality of the interface. An electrochemical DNA biosensor was further constructed using the composite film of PIA and eh-CdS as the supporting platform. Hybridization experiments showed that the target DNA could be quantified over a wide range from  $1.0 \times 10^{-14}$  to  $1.0 \times 10^{-9}$  M with a detection limit of  $3.9 \times 10^{-15}$  M.

## 2. Experimental

### 2.1. Reagents

IA and Tris (hydroxymethyl) aminomethane (Tris) were provided by Aladdin Reagent Company (China). 1-ethyl-3-(3-dimethylaminopropyl) carbodiimide (EDC) and N-hydroxysulfosuccinimide (NHS) were purchased from Sigma-Aldrich Co., Ltd. (China). MB was supplied by Shanghai Chemical Reagent Company (China). Phosphate buffer saline (PBS) was purchased from Shanghai Kang-Yi Instruments Co., Ltd. (China). Cadmium sulfate octahydrate ( $3\text{CdSO}_4 \cdot 8\text{H}_2\text{O}$ ), TU and Ethylenediaminetetraacetic acid (EDTA) were obtained from Xilong Chemical Co., Ltd. (China). All the other chemicals were analytical reagent grade and purchased commercially. Doubly distilled water (DDW) was used throughout the experiments.

The 24-base DNA fragments from *colitoxin* (Cai et al., 2003) were synthesized by Shanghai Sangon Bioengineering Co., Ltd. (China). Their base sequences are as follows:

- Probe sequence (S1): 5'-NH<sub>2</sub>-(CH<sub>2</sub>)<sub>6</sub>-GAG CGG CGC AAC ATT TCA GGT CGA-3'.
- Complementary sequence (S2): 5'-TCG ACC TGA AAT GTT GCG CCG CTC-3'.
- One-base mismatched sequence (S3): 5'-TCG ACC TGA AAT GTT GCG CCT CTC-3'.
- Three-base mismatched sequence (S4): 5'-TCG TCC TGA AAC GTT GCG CCT CTC-3'.
- Non-complementary sequence (S5): 5'-GCA CGG CGC AAC ATT TCA GGT CGA-3'.

Stoke solutions (10  $\mu\text{M}$ ) of all oligonucleotides were prepared with TE buffer solution (10  $\mu\text{M}$  Tris-HCl, 1.0 mM EDTA, pH 8.0) and kept frozen.

### 2.2. Apparatus

The size and morphology of the products were characterized by Hitachi S-4800 scanning electron microscopy (SEM, Japan). Atomic

force microscope (AFM) images were obtained with a CSPM 5500 scanning probe microscope (China). The cyclic voltammetry (CV), electrochemical impedance spectra (EIS) and differential pulse voltammetry (DPV) were carried out on a CHI 650D electrochemical station (China) with the conventional three-electrode system consisted of bare glassy carbon electrode (GCE,  $\Phi=2$  mm) or modified GCE as working electrode, Ag/AgCl as reference electrode and platinum wire as auxiliary electrode.

### 2.3. Preparation of CdS with different shapes

To 27 mL DDW containing 0.008 g TU, different amounts of  $3\text{CdSO}_4 \cdot 8\text{H}_2\text{O}$  was slowly added under stirring. Then the resulting homogeneous solution was transferred into a stainless steel autoclave (30.0 mL) of its 90% capacity of the total volume, sealed and maintained at 160 °C for 24 h. Afterwards, the autoclave was allowed to cool at room temperature. The yellow precipitates were centrifuged and completely washed with absolute ethanol and DDW in turn to obtain the pure products.

### 2.4. Step-by-step modification of GCE with CdS and PIA

Prior to modification, the GCE was polished to a mirror-like surface with 1.0, 0.3 and 0.05  $\mu\text{m}$  alumina slurry, and then successively washed with anhydrous ethanol and DDW for 3 min under ultrasonication. 1.0 mg of prepared CdS was dispersed in 10 mL of DDW with the aid of ultrasonic agitation to obtain a yellow suspension. Followed by, 10  $\mu\text{L}$  of above prepared CdS aqueous solution was dripped onto the fresh GCE surface and left to dry at room temperature. After careful washing with water, the CdS modified GCE (CdS/GCE) was fabricated. The electro-polymerization of IA was achieved by dipping CdS/GCE into 0.1 M KCl solution containing 0.1 mM IA and then scanned for 18 cycles in the potential range from 0 to +2.0 V with the scan rate of 60  $\text{mV s}^{-1}$ . After the scan was finished, a layer of uniform and bright-green membrane was observed on the electrode surface.

### 2.5. Probe DNA immobilization and hybridization

The amino-functionalized probe DNA was covalently attached on the surface of PIA/eh-CdS/GCE by the standard EDC/NHS cross-linking reaction. Briefly, immersing PIA/eh-CdS/GCE into 25 mM PBS containing 8 mM NHS and 5 mM EDC for 25 min, and then transferred into 1.0 mL TE buffer solution containing 0.1  $\mu\text{M}$  S1 at room temperature for 12 h. After sufficient rinsing with TE buffer and DDW to remove the physically absorbed DNA, the probe DNA modified electrode (S1/PIA/eh-CdS/GCE) was achieved. The hybridization reaction was performed by incubating S1/PIA/eh-CdS/GCE in TE buffer solution that contained desired concentration of S2 for 40 min at 42 °C, followed by washing with TE buffer to remove the unhybridized DNA. The resulted electrode was denoted as S2-S1/PIA/eh-CdS/GCE. The hybridizations of the probe DNA with the other control sequences including one-base mismatched DNA (S3), the three-base mismatched DNA (S4) and the non-complementary DNA (S5) were performed through the similar procedure, and the obtained electrodes were termed as S3-S1/PIA/eh-CdS/GCE, S4-S1/PIA/eh-CdS/GCE and S5-S1/PIA/eh-CdS/GCE, respectively.

### 2.6. Electrochemical measurements

The DNA immobilization and hybridization were monitored using MB as the redoxactive probe according to the following procedures: first, the DNA modified electrode was immersed into 50  $\mu\text{M}$  MB solution for 25 min, and then rinsed with PBS for 5 min and subsequently electrochemically measured in PBS solution with CV and differential pulse voltammetry (DPV) in the potential range

from  $-0.6$  V to  $0$  V. The fabrication and detection processes of the biosensor are illustrated in Scheme 1.

### 3. Results and discussion

#### 3.1. Morphologies of the synthesized CdS

Fig. 1 shows the SEM images of the synthesized products through reacting TU and  $\text{Cd}^{2+}$  with the molar ratios of 4:1 (A), 6:1 (B), and 12:1 (C). As seen, when TU was in a low content in the reaction solution, the CdS particles were not uniform and regular. The sizes of the irregular CdS particles (iCdS) showed a wide range from about  $300$  nm to  $2.0$   $\mu\text{m}$  (Fig. 1A). When the mole ratio of TU and  $\text{Cd}^{2+}$  was increased to 6:1, some rod-like CdS (rCdS) particles with diameter of about  $200$  nm began to appear, which was distributed among some aggregated CdS irregular particles (Fig. 1B). When the ratio of TU to  $\text{Cd}^{2+}$  was further increased to 12:1, it was interestingly found the shape of the products became very uniform and organized, and the irregular and uneven particles were almost absolutely disappeared (Fig. 1C). From the locally amplified image (Fig. 1D), it could be seen that CdS displayed unique elongated hexagonal-pyramid, in which the long axis perpendicular to the hexagonal plane. The typical structure of the eh-CdS was in the range from  $400$  to  $700$  nm in diameters and the length was about  $2.0$   $\mu\text{m}$ . This variation indicated that the content of the TU played an important role in the transformation of CdS material from the irregular form to the uniform rod-like shape and finally to the elongated hexagonal-pyramid shape. The possible mechanism is proposed as follows: when TU was in a low content,  $\text{S}^{2-}$  that slowly generated from the thermal decomposition of TU at  $160$   $^{\circ}\text{C}$  was rapidly adsorbed with large amount of  $\text{Cd}^{2+}$ , resulting in the amorphous precipitate of CdS. When  $\text{S}^{2-}$  was increased with the increase of TU content, the excessive amount of  $\text{S}^{2-}$  was selectively bound to specific crystallographic facets of preliminarily formed CdS nanocrystals, therefore leading to the anisotropic growth of the crystals. Fig. 1E shows the XRD pattern of the as synthesized eh-CdS nanoparticles. The strong and sharp diffraction peaks indicated that the sample was well crystallized. All the diffraction peaks can be indexed as wurtzite CdS with lattice constant of  $a=b=4.136$   $\text{\AA}$  and  $c=6.713$   $\text{\AA}$ , which are in good agreement with the literature values (JCPDS Card no. 77-2306) (Shen et al., 2005). Compared to the standard reflection, the intensity of the (002) diffraction peak of the sample was comparatively strong, which indicated the preferential crystal growth orientation along the  $c$ -axis (Wang et al., 2011b). Also, no peaks

of impurities were detected, revealing high purity of the as-synthesized products.

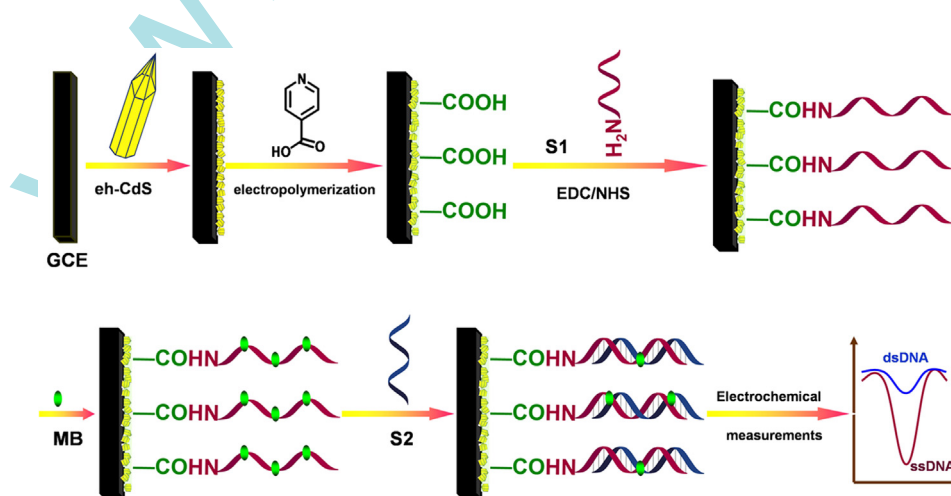
#### 3.2. Electro-polymerization of IA on eh-CdS/GCE and the AFM characterization

Electro-polymerization is facile and economical approach to introduce the functional film onto the electrode interface. In this work, the IA was used as the monomer to polymerize on CdS modified electrode through an electrochemical method. Fig. S1 in Supplementary material shows the continuously scanned CVs of  $1.0 \times 10^{-4}$  M IA on eh-CdS/GCE over the range from  $0$  to  $+2.0$  V at  $60$   $\text{mV s}^{-1}$ . As seen, increasing oxidation peaks were observed at  $+0.5$  V with successional scanning, which reflected the continuous growth of the film on the electrode surface. When the cyclic sweep was scanned up to the 18th cycle, the peaks were hardly changed, suggesting that the polymerized film had been saturated eh-CdS/GCE. In addition, it was found that after the electro-polymerization process was ended, a layer of uniform and bright-green film was observed on the surface of the modified electrode, further indicating that PIA has been successfully electrodeposited on the surface of eh-CdS/GCE.

The AFM technique was also employed to confirm the formation of PIA on the electrode surface. Fig. 2 shows the three dimensional (a) and cross-sectional (b) images of GCE (A), eh-CdS/GCE (B) and PIA/eh-CdS/GCE(C). It was observed that the bare GCE is relatively flat and smooth with the largest peak height of only  $8.66$  nm (Fig. 2A). The average roughness ( $R_a$ ) was determined to be  $1.65$  nm. After eh-CdS was cast on the bare GCE, many adjacent broad peaks with the average height of  $250.03$  nm were determined (Fig. 2B) and the  $R_a$  value was accordingly increased to  $27.81$  nm. This variation suggested that the material of eh-CdS had been attached on GCE surface. Furthermore, when PIA/eh-CdS/GCE was measured, it was found that some uniform and order peaks were appeared, and the average height and  $R_a$  value further increased to  $344.56$  nm and  $49.32$  nm (Fig. 2C), respectively, testifying that the PIA had been successfully grown on eh-CdS/GCE.

#### 3.3. Electrochemical characteristics of the modified electrodes

The electrochemical property of PIA/eh-CdS film and its application as a supporting platform for DNA immobilization were probed by CV (Fig. 3A) and EIS (Fig. 3B) using  $[\text{Fe}(\text{CN})_6]^{3-/4-}$  as the redox probe. In the CV experiments, it was observed that the bare GCE presented a pair of well-defined redox peaks in  $[\text{Fe}(\text{CN})_6]^{3-/4-}$  solution (curve a). When the eh-CdS modified GCE was applied for measurement, it was



Scheme 1. Illustration for the fabrication procedures of the eh-CdS/PIA composite film based DNA biosensor.

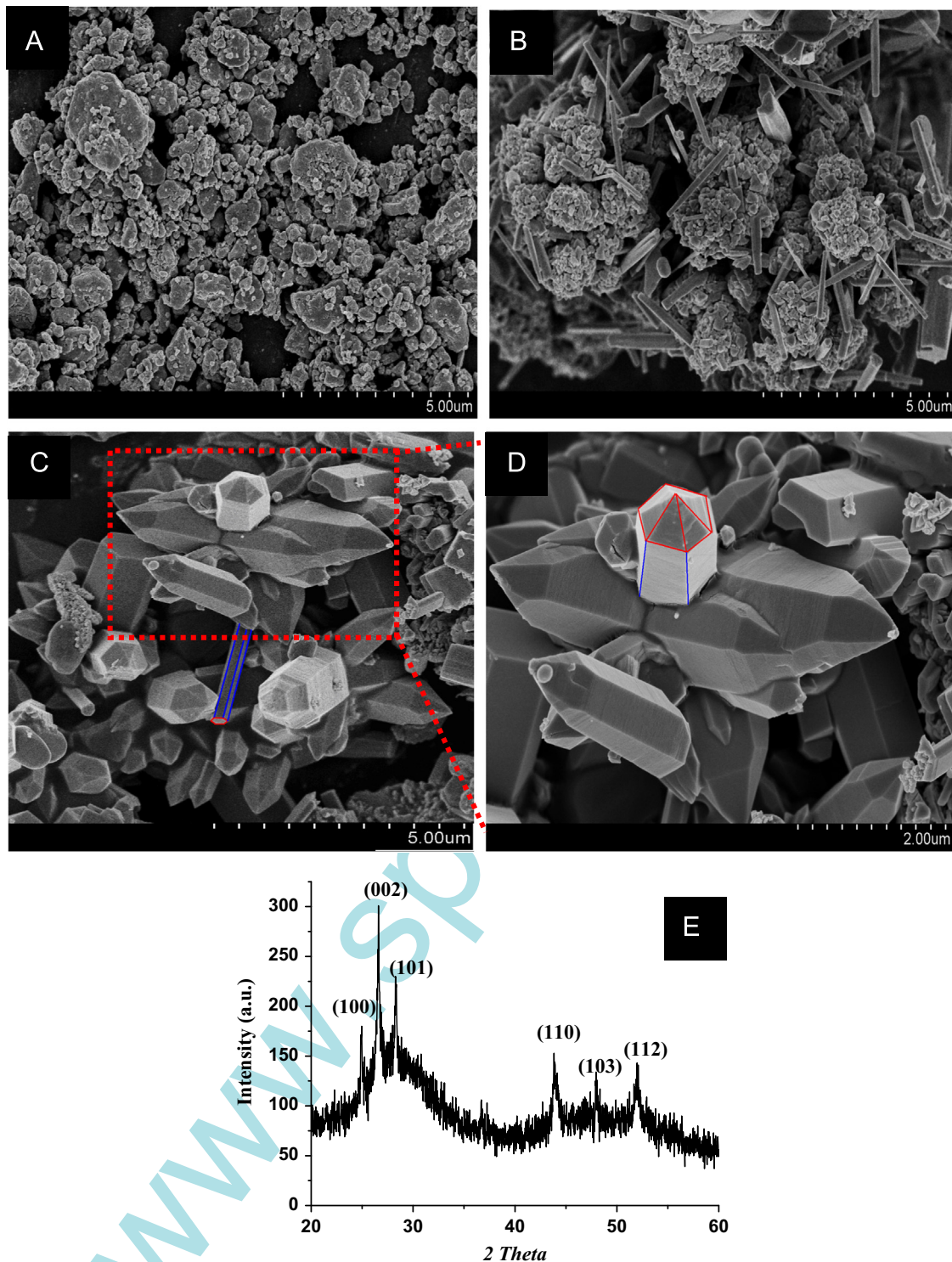


**Fig. 1.** SEM images of CdS synthesized with the molar ratio of Cd<sup>2+</sup> to TU at 1:4 (A), 1:6 (B) and 1:12 (C), and the partial magnification of image C (D). (E) XRD pattern of the eh-CdS nanoparticles.

found that the electrochemical response of  $[\text{Fe}(\text{CN})_6]^{3-/4-}$  was significantly enhanced (curve b), which indicating that the eh-CdS nanoparticles had remarkable electrocatalysis owing to its semiconductive property. However on GCE directly electropolymerized with PIA (PIA/GCE), the redox peaks of  $[\text{Fe}(\text{CN})_6]^{3-/4-}$  were almost disappeared (curve c). This indicated that the single film of PIA had inferior electrical conductivity. While on PIA/eh-CdS/GCE, it was found that the electrochemical response of  $[\text{Fe}(\text{CN})_6]^{3-/4-}$  was greatly enhanced (curve d) in comparison with PIA/GCE. This further

confirmed that the eh-CdS could be acted as an excellent electron transfer pathway in the composite film. Nevertheless, it was found that when eh-CdS/GCE was repeatedly scanned in  $[\text{Fe}(\text{CN})_6]^{3-/4-}$  solution, the obtained electrochemical response decreased gradually with the increase of the scan time; but the response on PIA/eh-CdS/GCE was almost constant. This difference indicated that PIA/eh-CdS/GCE had much higher stability than eh-CdS/GCE during electrochemical measurements, which could be explained by the fact that stable PIA film could effectively prevent the falling away of eh-CdS from GCE

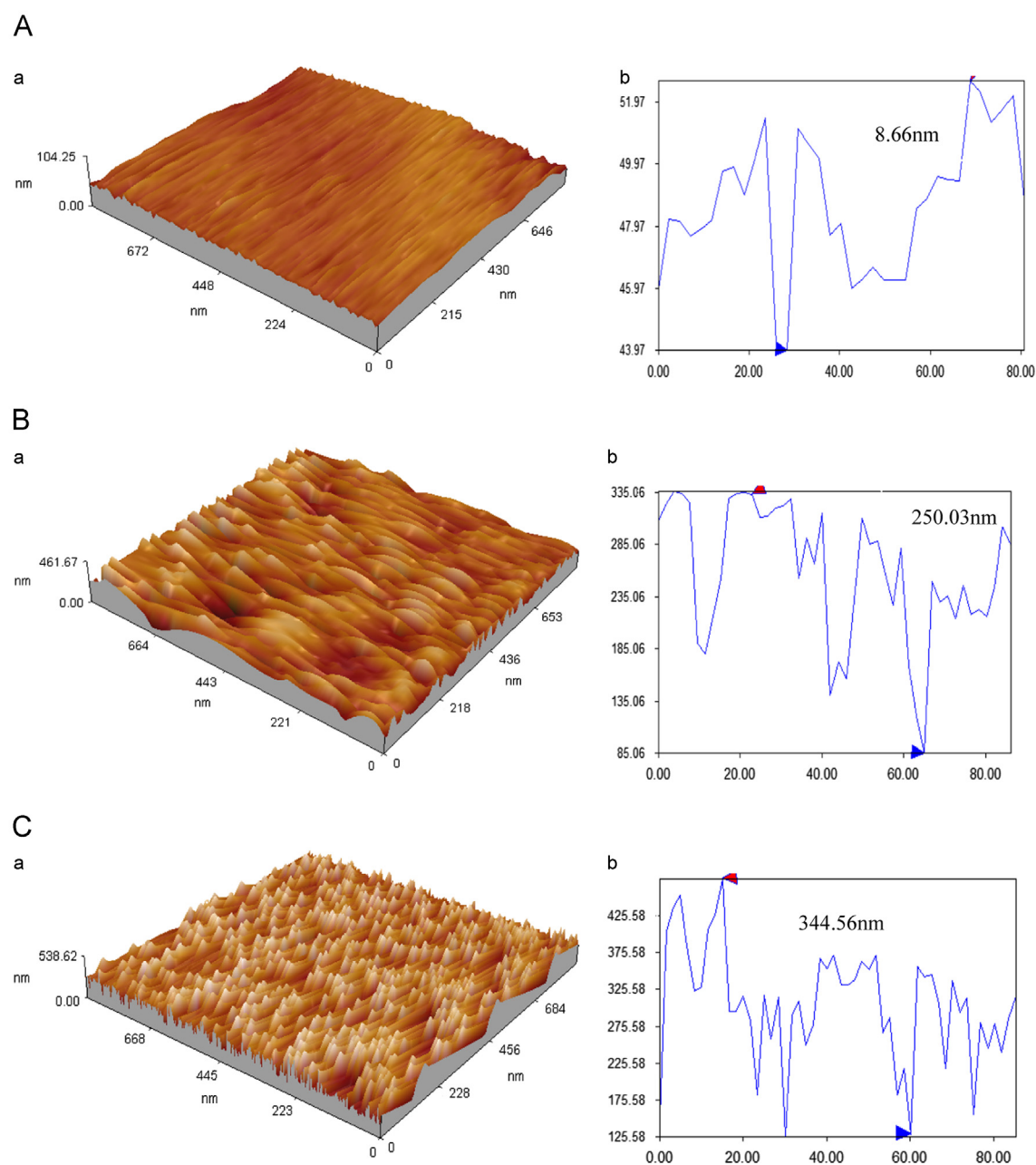


Fig. 2. AFM images of three dimensional (a) and cross-sectional (b) graphs of bare GCE (A), eh-CdS/GCE (B) and PIA/eh-CdS/GCE (C).

surface. Therefore it could be concluded that the composite film of PIA/eh-CdS combined the advantages of each component, i.e., the high stability of PIA and excellent electrical conductivity of eh-CdS. Moreover, according to the Randles–Sevcik equation (Xiao et al., 2008):

$$I_{pc} = (2.69 \times 10^5) n^3/2 AD^{1/2} C v^{1/2}$$

where  $I_{pc}$  is the reduction peak current (A),  $n$  the electron transfer number,  $A$  the accessible active surface area ( $\text{cm}^2$ ),  $D$  the diffusion coefficient of  $[\text{Fe}(\text{CN})_6]^{3-}$  in the solution ( $\text{cm}^2 \text{s}^{-1}$ ),  $C$  the concentration of  $[\text{Fe}(\text{CN})_6]^{3-}$  (M) and  $v$  the scan rate ( $\text{V s}^{-1}$ ), the accessible active surface area ( $A$ ) of different electrodes can be calculated. From

the CV results displayed in Fig. 3A, the values of  $A$  of PIA/GCE and PIA/eh-CdS/GCE were calculated to be 0.002 and 0.027  $\text{cm}^2$ , respectively, which suggested that the presence of eh-CdS nanoparticles increased the accessible area of the electrode by about 13.5-fold due to the nanometer size effect of eh-CdS.

In addition, the covalent immobilization of probe DNA on the nanocomposite modified electrode under the aid of EDC/NHS was also characterized, and the results were depicted as curve e in Fig. 3A. As seen, the redox peaks of  $[\text{Fe}(\text{CN})_6]^{3-/4-}$  decreased obviously as compared to those on PIA/eh-CdS/GCE, suggesting that probe DNA had been successfully anchored on PIA/eh-CdS/GCE.

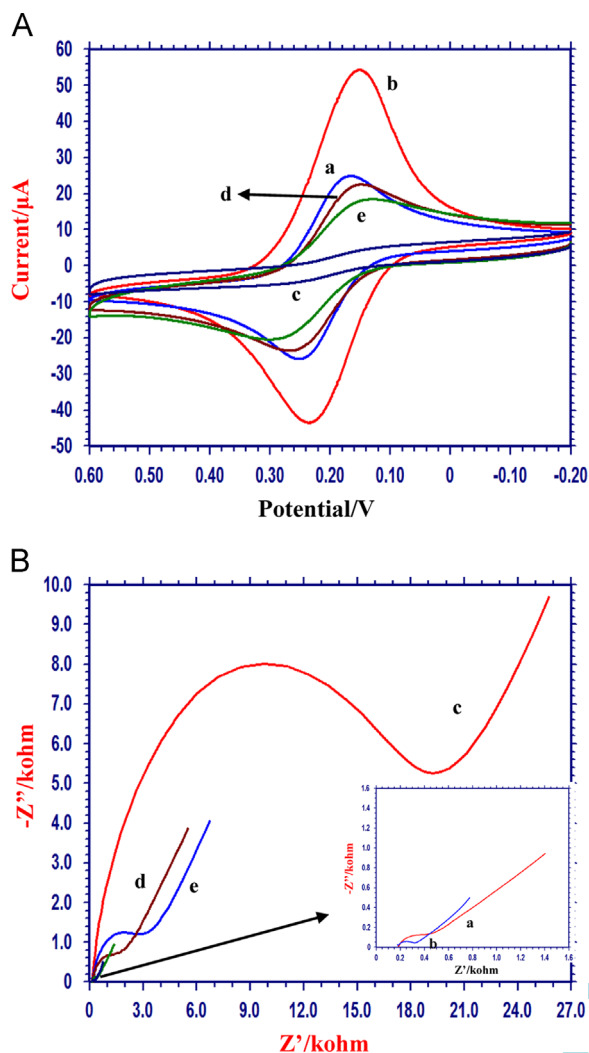


**Fig. 3.** CVs (A) and EIS (B) of bare GCE (a), eh-CdS/GCE (b), PIA/GCE (c), PIA/eh-CdS/GCE (d) and S1/PIA/eh-CdS/GCE (e) in 1.0 mM  $[\text{Fe}(\text{CN})_6]^{3-/4-}$  containing 0.1 M KCl.

This was because the negatively charged of phosphate backbone on the probe DNA interfered the diffusion of electronegative  $[\text{Fe}(\text{CN})_6]^{3-/4-}$  to the electrode surface.

Electrochemical impedance spectroscopy (EIS) has been proved as a very powerful tool for investigating the interfacial properties of conductive or semi-conductive surfaces (Gao et al., 2011). In EIS, the semicircle diameter at the higher frequencies equals to the electron transfer resistance ( $R_{\text{et}}$ ) that controls the electron transfer kinetics of the redox probes. In this work, the modified processes are also characterized by EIS and the obtained Nyquist plots are presented in Fig. 3B. It could be found that the  $R_{\text{et}}$  value on eh-CdS/GCE (curve b) was obviously smaller than the bare GCE (curve a), which also demonstrated that the eh-CdS nanoparticles accelerated the electron transfer kinetics of the electrode surface. In contrast, the  $R_{\text{et}}$  value on PIA/GCE was significantly increased (curve c) as compared with bare GCE, suggesting that the electron transfer process of  $[\text{Fe}(\text{CN})_6]^{3-/4-}$  was inhibited by the single-component film of PIA. However on PIA/eh-CdS/GCE, the  $R_{\text{et}}$  value was decreased again (curve d), further testifying that the eh-CdS nanoparticles could effectively catalyze the electron transfer process of the composite film. Upon immobilization of S1 on PIA/eh-CdS/GCE, the  $R_{\text{et}}$  value increased again due to the electrostatic repulsion of the immobilized DNA to  $[\text{Fe}(\text{CN})_6]^{3-/4-}$  ions (curve e).

The structure-property (electrocatalysis)-relationship in electrochemistry of the three synthesized CdS with different shapes

was also evaluated by EIS. The Nyquist diagrams of PIA/GCE (a), PIA/eh-CdS/GCE (b), PIA/rCdS/GCE (c) and PIA/iCdS/GCE (d) in 1.0 mM  $[\text{Fe}(\text{CN})_6]^{3-/4-}$  solution with 0.1 M KCl are shown in Fig. S2 in Supplementary material. Through comparison, it could be clearly observed that the  $R_{\text{et}}$  value on PIA/GCE ( $2.0 \times 10^4 \Omega$ , curve a) was larger than those on PIA/eh-CdS/GCE ( $2.0 \times 10^3 \Omega$ , curve b), PIA/rCdS/GCE ( $4.5 \times 10^3 \Omega$ , curve c) and PIA/iCdS/GCE ( $6.5 \times 10^3 \Omega$ , curve d), suggesting that all the CdS nanoparticles with different morphologies had the electrocatalysis to the electroactive molecules. Moreover, it could be found that with the particles becoming more irregular in shape, the electrical conductivity becomes better as judged from the smaller  $R_{\text{et}}$  values. This also indicated that the shape and surface structure could effectively control the electrochemical property of the materials. Das and Raj (2013) had reported that the polyhedral nanoparticles had the higher electrocatalytic activity than the other forms since it possessed much more electrocatalytic sites. Therefore, we deduced that the polyhedral eh-CdS prepared in this work had the similar feature. Therefore in the following DNA sensing experiments, only PIA/eh-CdS/GCE was investigated because it had the best electrocatalytic property.

### 3.4. Electrochemical behaviors of MB at modified electrodes

MB is a typical redox-active phenothiazine dye, which has been frequently used as an electrochemical indicator to probe DNA immobilization and hybridization based on its specific affinity with the unpaired guanine bases (Sun et al., 2010; Qi et al., 2012). In order to investigate the electrochemical sensing property of the developed biosensor, the electrochemical behaviors of MB on the biosensor were further investigated. Fig. S3 in Supplementary material shows the DPVs of MB at S1/PIA/eh-CdS/GCE with different accumulation time. Obviously, with increase of the accumulation time, the electrochemical signals of MB increased gradually, suggesting that increasing amount of MB had been bound to the electrode surface through interaction with probe DNA. When the time was up to 25 min, the DPV peaks of MB became constant, showing the saturation of MB at the electrode surface. Thus 25 min was chosen as the optimal time for MB accumulation to achieve the highest sensitivity of biosensor.

Fig. 4A shows the typical CVs of sufficiently pre-accumulated MB on PIA/eh-CdS/GCE, S1/PIA/GCE and S1/PIA/eh-CdS/GCE. It was observed that a pair of tiny redox peaks were appeared on PIA/eh-CdS/GCE (curve a), suggesting that only small amount of MB was absorbed on the electrode. However on S1/PIA/eh-CdS/GCE, a pair of dramatically increased redox peak of MB was observed (curve c), demonstrating that much more MB molecules had been adsorbed, which could be ascribed to the specific interaction of MB with the immobilized DNA (Sun et al., 2010; Qi et al., 2012). As a control, the electrochemical behavior of MB on S1/PIA/GCE was also investigated, and the result (curve b) revealed that the peak intensity on this electrode was much smaller than that on S1/PIA/eh-CdS/GCE. This confirmed that the presence of eh-CdS was more favorable to enhance the electrochemical sensitivity of the biosensor. Fig. 4B shows the influence of scan rate ( $\nu$ ) on the redox peak current of MB at S1/PIA/eh-CdS/GCE. With the increase of scan rate, both reduction peak currents ( $I_{\text{pc}}$ ) and oxidation peak currents ( $I_{\text{pa}}$ ) increased gradually, and showed good linearity with the scan rate in the range from 60 to 450  $\text{mV s}^{-1}$  with the linear regression equations of  $I_{\text{pa}}/10^{-6} \text{ A} = -41.87 \nu(\text{mV s}^{-1}) - 0.0718$  ( $r = -0.999$ ) and  $I_{\text{pc}}/10^{-6} = 42.24 \nu(\text{mV/s}) + 1.397$  ( $r = 0.998$ ) (inset of Fig. 4B), further suggesting that the redox indicator of MB had been bound to S1/PIA/eh-CdS/GCE.

In addition, according to the facile method provided by Zhang et al. (2008), the surface density of probe DNA ( $\Gamma$ ) anchored on the electrode surface was calculated. First, from the CV curve of MB on

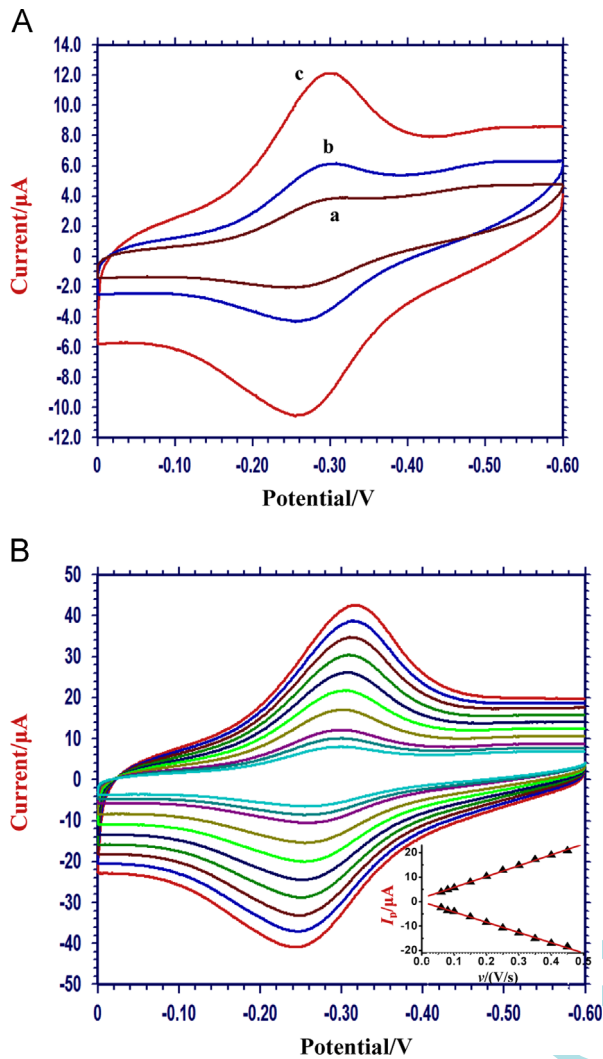


**Fig. 4.** (A) CVs of MB at PIA/eh-CdS/GCE (a), S1/PIA/GCE (b), and S1/PIA/eh-CdS/GCE (c) in 0.1 M PBS (pH 7.0). (B) Dependence of CVs of MB at S1/PIA/eh-CdS/GCE on scan rate ( $\nu$ ). From inner to outer: 60, 80, 100, 150, 200, 250, 300, 350, 400 and 450  $\text{mV s}^{-1}$ . Inset shows the plots of  $I_{pa}$  and  $I_{pc}$  versus  $\nu$ .

the biosensor, the charge quantity ( $Q$ ) of MB was obtained to be  $1.8 \times 10^{-5}$  C, which corresponded to the molar quantity ( $N$ ) of  $9.4 \times 10^{-11}$  mol as calculated according to the equation of  $N = Q/neN_A$ , where  $n$  ( $=2$ ) is the number of electrons participating in the electrode reaction of MB;  $e$  ( $=1.6 \times 10^{-19}$  C) the charge quantity of one electron;  $N$  ( $=6.02 \times 10^{23} \text{ mol}^{-1}$ ) Avogadro's number. Meanwhile, because MB molecule combined with guanine base via the stoichiometric ratio of 1:1, and every DNA probe strand contained eight guanine bases, the immobilized amount of DNA on the electrode surface was determined as  $1.2 \times 10^{-11}$  mol. When the electrode surface area was further considered, the value of  $\Gamma$ , i.e., the surface density of probe DNA of the biosensor was estimated to be  $4.35 \times 10^{-10} \text{ mol cm}^{-2}$  (or  $2.62 \times 10^{14}$  molecules  $\text{cm}^{-2}$ ), which was larger than the values on bare matrix-based DNA biosensors (Peterson et al., 2001; Steel et al., 1998) and also on the nonmaterial based biosensors that fabricated through non-covalently physical absorption (Zhang et al., 2008; Yang et al., 2011).

### 3.5. Analytical performance of the biosensor

Fig. 5A shows the DPVs of MB on S1/PIA/eh-CdS/GCE upon hybridization with different concentrations of fully matched DNA sequence (S2). As seen, with the increase of the S2 concentration ( $C_{S2}$ )

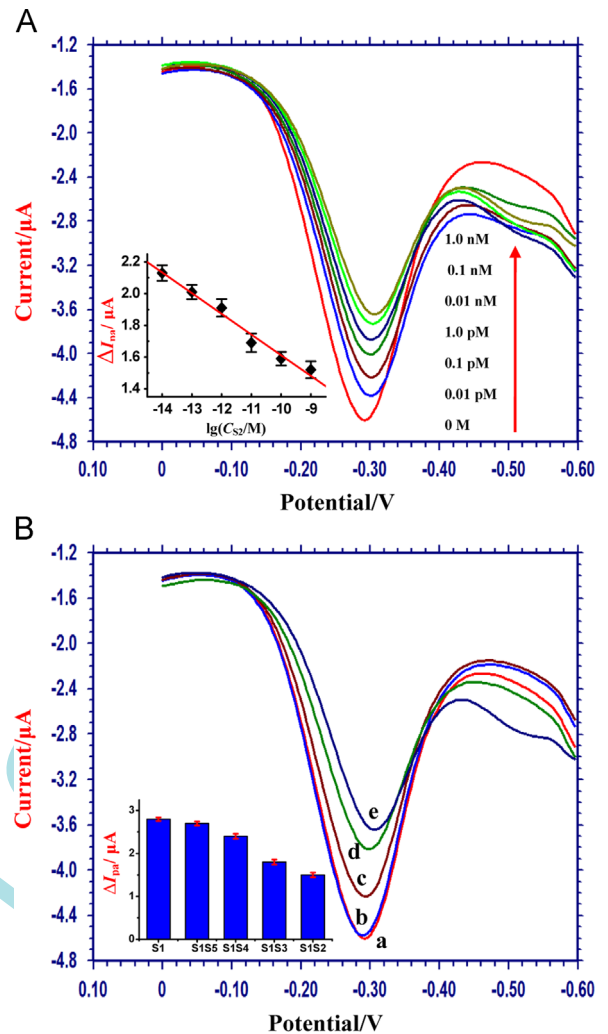


**Fig. 5.** (A) DPVs of MB at S1/PIA/eh-CdS/GCE upon hybridization with increasing amounts of S2. Inset shows the plot of  $\Delta I_{pa}$  versus the logarithm values of  $C_{S2}$  ( $\lg C_{S2}$ ). (B) DPVs of MB at the biosensor before (a) and after hybridization with the complementary (e), the non-complementary (b), single-base mismatched (d) and three-base mismatched (c) sequences. Inset shows the corresponding histogram.

in the hybridization solution, the  $I_{pa}$  values of MB decreased gradually, suggesting that much more double-helix structured DNA had been formed on the biosensor. When the difference ( $\Delta I_{pa}$ ) of  $I_{pa}$  before and after hybridization was utilized as the sensing signal, it was found that  $\Delta I_{pa}$  showed a good linearity with the logarithmic values of  $C_{S2}$  ( $\lg C_{S2}$ ) in a wide range from  $1.0 \times 10^{-14}$  to  $1.0 \times 10^{-9}$  M (inset of Fig. 5A). The linear regression equation was  $\Delta I_{pa}/10^{-5} \text{ A} = 0.335 - 0.128 \lg(C_{S2}/\text{M})$  ( $r^2 = 0.995$ ). Based on  $3\sigma$  (where  $\sigma$  is the relative standard deviation of the blank solution,  $n=7$ ), a low detection limit of  $3.9 \times 10^{-15}$  M was estimated. Table S1 in Supplementary material lists the detection limits and linear ranges of different DNA biosensors in hybridization detection. Through comparison, it could be found that the DNA biosensor proposed in our work exhibited the comparable or better analytical performance than the others.

The hybridization selectivity of the biosensor was also evaluated by hybridization with different sequences including the complementary DNA sequence, the non-complementary sequence, single-base mismatched sequence and three-base mismatched sequence. The DPV results are shown in Fig. 5B. It was observed that the highest DPV signal of MB was obtained at the S1/PIA/eh-CdS/GCE (curve a), owing to the strong affinity of MB to the free guanine bases of probe DNA. A significant decrease of DPV signal

was observed after the biosensor was hybridized with the complementary target sequences S2 (curve e). However, the variation of the DPV curve of MB was negligible after the biosensor was hybridized with the non-complementary sequences S5 (curve b), indicating that hybridization reaction did not occur. Moreover, when the biosensor was hybridized with the single-base mismatched S3 (curve d) and the three-base mismatched S4 (curve c), the decreases of the oxidative DPV peaks were much smaller than that obtained on the S2 hybridized electrode, suggesting that only partial hybridizations occurred for these two DNA sequences. In addition, the two mismatched sequences could be well recognized via comparing the decrease degree of the peak current values of MB on the two hybridized electrodes. All these results demonstrated that the fabricated DNA biosensor had high selectivity for the hybridization detection.

#### 4. Reproducibility and stability of the biosensor

The reproducibility and stability are extremely important for a biosensor in practical applications. The reproducibility of the developed biosensor was monitored by detecting  $1.0 \times 10^{-9}$  M target DNA with six parallel-made S1/PIA/eh-CdS/GCE. The results showed that a relative standard deviation (R.S.D.) of 3.26% ( $n=6$ ) was estimated, showing a high reproducibility of the constructed DNA biosensor. The stability experiment showed that storage of S1/PIA/eh-CdS/GCE at 4 °C for two weeks only resulted in a change of 5.1% in the initial  $R_{et}$  response, suggesting a good stability of the biosensor.

#### 5. Conclusions

In this work, three CdS materials with different shapes were facilely synthesized through tuning the molar ratio of  $Cd^{2+}$  to TU. The electrochemical characterization experiments showed that CdS with elongated hexagonal-pyramid shape had the highest electrocatalytic property. Then a novel DNA biosensor was fabricated using eh-CdS with electrosynthesized PIA as the probe supporting materials. The composite film of eh-CdS/PIA provided rich functional groups with large surface area for probe DNA immobilization. The high sensitivity of the biosensor for the detection of target DNA was achieved with a wide dynamic range from  $1.0 \times 10^{-14}$  M to  $1.0 \times 10^{-9}$  M and a low detection limit of  $3.9 \times 10^{-15}$  M. Moreover, the reported biosensor had impressive selectivity with successful discrimination of the target DNA from other sequences. These results demonstrated the potential of the biosensor to meet the need for the inexpensive, accurate, and hand-held detection of DNA.

#### Acknowledgments

The work is supported by the National Natural Science Foundation of China (No. 21275127), Program for New Century Excellent Talents in Fujian Province University (No. JA12204), and Key Research Foundation of Fujian Education Department (No. JA11166).

#### Appendix A. Supporting information

Supplementary data associated with this article can be found in the online version at <http://dx.doi.org/10.1016/j.bios.2014.04.011>.

#### References

- Ameen, S., Akhtar, M.S., Kim, Y.S., Shin, H.S., 2012. *Chem. Eng. J.* 181–182, 806–812.
- Cai, H., Zhu, N.N., Jiang, Y., He, P.G., Fang, Y.Z., 2003. *Biosens. Bioelectron.* 18, 1311–1319.
- Das, A.K., Raj, C.R., 2013. *Electrochim. Acta* 107, 592–598.
- Du, P., Li, H.X., Mei, Z.H., Liu, S.F., 2009. *Bioelectrochemistry* 75, 37–43.
- Fang, Y.M., Sun, J.J., Wu, A.H., Su, X.L., Chen, G.N., 2009. *Langmuir* 25, 555–560.
- Ferancová, A., Rengaraj, S., Kim, Y., Labuda, J., Sillanpää, M., 2010. *Biosens. Bioelectron.* 26, 314–320.
- Gao, H.W., Qi, X.W., Chen, Y., Sun, W., 2011. *Anal. Chim. Acta* 704, 133–138.
- Huang, Y.X., Zhang, W.J., Xiao, H., Li, G.X., 2005. *Biosens. Bioelectron.* 21, 817–821.
- Liu, Y.H., Li, H.N., Chen, W., Liu, A.L., Lin, X.H., Chen, Y.Z., 2013. *Anal. Chem.* 85, 273–277.
- Long, Y.F., Jiang, D.L., Zhu, X., Wang, J.X., Zhou, F.M., 2009. *Anal. Chem.* 81, 2652–2657.
- Lou, X.H., Zhao, T., Liu, R., Ma, J., Xiao, Y., 2013. *Anal. Chem.* 85, 7574–7580.
- Miao, X.M., Yuan, R., Chai, Y.Q., Shi, Y.T., Yuan, Y.R., 2008. *Biochem. Eng. J.* 38, 9–15.
- Ojani, R., Raouf, J.B., Norouzi, B., 2011. *J. Solid State Electrochem.* 15, 1139–1147.
- Peng, H., Zhang, L.J., Soeller, C., Travas-Sejdic, J., 2009. *Biomaterials* 30, 2132–2148.
- Peterson, A.W., Heaton, R.J., Georgiadis, R.M., 2001. *Nucl. Acids Res.* 29, 5163–5168.
- Qi, X.W., Gao, H.W., Zhang, Y.Y., Wang, X.Z., Chen, Y., Sun, W., 2012. *Bioelectrochemistry* 88, 42–47.
- Qian, J.Q., Yan, S.C., Xiao, Z.D., 2012. *J. Colloid Interface Sci.* 366, 130–134.
- Sun, W., Qin, P., Gao, H.W., Li, G.C., Jiao, K., 2010. *Biosens. Bioelectron.* 25, 1264–1270.
- Steel, A.B., Herne, T.M., Tarlov, M.J., 1998. *Anal. Chem.* 70, 4670–4677.
- Wan, Y., Lao, R.J., Liu, G., Song, S.P., Wang, L.H., Li, D., Fan, C.H., 2010. *J. Phys. Chem. B* 114, 6703–6706.
- Wang, J., Shan, Y., Zhao, W.W., Xu, J.J., Chen, H.Y., 2011a. *Anal. Chem.* 83, 4004–4011.
- Wang, X.J., Zou, B.S., Zhang, Q.L., Lei, A.H., Zhang, W.J., Ren, P.Y., 2011b. *J. Alloys Compd.* 509, 9959–9963.
- Xiao, F., Zhao, F.Q., Li, J.W., Liu, L.Q., Zeng, B.Z., 2008. *Electrochim. Acta* 53, 7781–7788.
- Xuan, F., Luo, X.T., Hsing, I.M., 2012. *Anal. Chem.* 84, 5216–5220.
- Xue, H.G., Shen, Z.Q., Li, C.M., 2005. *Biosens. Bioelectron.* 20, 2330–2334.
- Yang, T., Feng, Y.Y., Zhang, W., Ma, S.Y., Jiao, K., 2011. *J. Electroanal. Chem.* 656, 140–146.
- Zhang, W., Yang, T., Jiang, C., Jiao, K., 2008. *Appl. Surf. Sci.* 254, 4750–4756.
- Zhang, Y.Y., Tang, Z.W., Wang, J., Wu, H., Maham, A., Lin, Y.H., 2010. *Anal. Chem.* 82, 6440–6446.
- Zhao, H., Zhang, Y.Z., Yuan, Z.B., 2002. *Anal. Chim. Acta* 454, 75–81.
- Zhu, X.H., Lin, X.Q., 2009. *Chin. J. Chem.* 27, 1103–1109.